INTERNATIONAL JOURNAL FOR NUMERICAL METHODS IN FLUIDS
Int. J. Numer. Meth. Fluids 2005; **47**:325–338
Published online 3 December 2004 in Wiley InterScience (www.interscience.wiley.com). DOI: 10.1002/fld.809

Low Reynolds number k–ε model for near-wall flow

M. M. Rahman*,† and T. Siikonen

Laboratory of Applied Thermodynamics, Department of Mechanical Engineering, Helsinki University of Technology, Sähkömiehentie 4, FIN-02015 HUT, Finland

SUMMARY

A wall-distance free k–ε turbulence model is developed that accounts for the near-wall and low Reynolds number effects emanating from the physical requirements. The model coefficients/functions depend non-linearly on both the strain rate and vorticity invariants. Included diffusion terms and modified $C_{\varepsilon(1,2)}$ coefficients amplify the level of dissipation in non-equilibrium flow regions, thus reducing the kinetic energy and length scale magnitudes to improve prediction of adverse pressure gradient flows, involving flow separation and reattachment. The model is validated against a few flow cases, yielding predictions in good agreement with the direct numerical simulation (DNS) and experimental data. Copyright © 2005 John Wiley & Sons, Ltd.

KEY WORDS: wall distance; near-wall turbulence; cross-diffusion; non-equilibrium flow

1. INTRODUCTION

The predictive capability of the complex turbulent flows encountered in engineering applications can be substantially enhanced by improved turbulence modelling. In principle, the high Reynolds number model is incapable of properly yielding near-wall resolution adhering to wall damping and viscous effects. Abandoning the wall function approach to patch near-wall regions, a large number of low Reynolds number (LRN) modifications have been proposed to two-equation turbulence closures where the integration up to the wall is extremely important. However, the modelling of near-wall turbulence in many existing LRN models usually involves distance to wall as an explicit parameter [1–6]. This renders the model often inappropriate to simulating flows with complex geometry, the wall distance of which becomes cumbersome to define. A remedy to this flaw is to develop a model which implicates no explicit wall distance while integrating it toward the solid surface [7–11]. The physical rationale behind the LRN model, independent of the wall topology, can be ascribed to nontrivial

*Correspondence to: M. M. Rahman, Laboratory of Applied Thermodynamics, Department of Mechanical Engineering, Helsinki University of Technology, Sähkömiehentie 4, FIN-02015 HUT, Finland.
†E-mail: mizanur.rahman@hut.fi

Received 7 March 2004
Revised 28 August 2004
Accepted 14 October 2004

suitability to wall functions and an achievable reduction in the programming/running time by integrating the LRN model to the wall [12].

An LRN k–ε turbulence model is developed, requiring no wall function/distance parameter that bridges the near-wall integration. To enhance dissipation in non-equilibrium flow regions, the model coefficients $C_{\varepsilon(1,2)}$ depend non-linearly on both the rotational and irrotational strains. The cross-diffusion terms in the ε transport equation reduce the turbulent kinetic energy and length scale magnitudes to improve prediction of adverse pressure gradient flows involving separation and reattachment. The wall singularity is removed by using an appropriate time scale that never falls below the Kolmogorov (dissipative eddy) time scale, representing the time scale realizability enforcement accompanied by the near-wall turbulent phenomena. An eddy viscosity damping function is designed in terms of total kinetic energy, and the invariants of strain rate and vorticity tensors. In addition, the turbulent Prandtl numbers $\sigma_{(k,\varepsilon)}$ are adjusted such as to provide substantial turbulent diffusion in near-wall regions. In essence, the model is tensorially invariant, frame-indifferent and applicable to arbitrary topologies.

The performance of the new model is demonstrated through the comparison with experimental and direct numerical simulation (DNS) data of well-documented flows, consisting of fully developed channel flows, a flat plate boundary layer flow with zero pressure gradient, and a backward facing step flow, respectively.

2. TURBULENCE MODEL

In collaboration with the Reynolds-averaged Navier–Stokes (RANS) equations, the proposed model determines the turbulence kinetic energy k and its dissipation rate ε by the following transport relations:

$$\frac{\partial \rho k}{\partial t} + \frac{\partial \rho U_j k}{\partial x_j} = \frac{\partial}{\partial x_j}\left[\left(\mu + \frac{\mu_T}{\sigma_k}\right)\frac{\partial k}{\partial x_j}\right] + P - \rho\varepsilon \tag{1}$$

$$\frac{\partial \rho \varepsilon}{\partial t} + \frac{\partial \rho U_j \varepsilon}{\partial x_j} = \frac{\partial}{\partial x_j}\left[\left(\mu + \frac{\mu_T}{\sigma_\varepsilon}\right)\frac{\partial \varepsilon}{\partial x_j}\right] + (C_{\varepsilon 1}P - C_{\varepsilon 2}\rho\varepsilon + E_\varepsilon)/T_t + \Pi_\varepsilon \tag{2}$$

where the turbulent production term $P = -\rho\overline{u_i u_j}(\partial U_i/\partial x_j)$ and E_ε is a secondary source term designed to increase the level of ε in non-equilibrium flow regions. The Reynolds stresses $\rho\overline{u_i u_j}$ are related to the mean strain rate tensor S_{ij} through the Boussinesq approximation. The symbolized Π_ε is the pressure diffusion term, balancing the molecular diffusion in the near-wall region [2, 13]. The eddy viscosity and the turbulence time scale are evaluated as

$$\mu_T = C_\mu f_\mu \rho k T_t, \quad T_t = \sqrt{\frac{k^2}{\varepsilon^2} + C_T^2\frac{v}{\varepsilon}} \tag{3}$$

where $C_\mu = 0.09$ and v represents the kinematic viscosity. The realizable time scale T_t prevents the singularity at $y_n = 0$ in the dissipation equation, where y_n is the normal distance from the wall. The empirical constant $C_T = \sqrt{2}$ associated with the Kolmogorov time scale is estimated from the behaviour of k in the viscous sublayer [3].

As a pragmatic device, the damping function f_μ is chosen to be a function of R_λ, given by

$$f_\mu = f_\lambda + C_v(1 - f_\lambda), \quad R_\lambda = \sqrt{\frac{C_\mu K_\mathrm{T}}{v\eta}}$$
$$f_\lambda = \tanh[C_\lambda R_\lambda(1 + R_\lambda)], \quad K_\mathrm{T} = \mathbf{U}\cdot\mathbf{U}/2 + k \tag{4}$$

where $C_\lambda = \beta C_\mu^{C_{\varepsilon 2}}$, $\beta = C_v T_t \eta$ and $\eta = \max(S, W)$, containing the invariants $S = \sqrt{2S_{ij}S_{ij}}$ and $W = \sqrt{2W_{ij}W_{ij}}$. The mean strain rate and mean vorticity tensors S_{ij} and W_{ij}, respectively, are defined as

$$S_{ij} = \frac{1}{2}\left(\frac{\partial U_i}{\partial x_j} + \frac{\partial U_j}{\partial x_i}\right), \quad W_{ij} = \frac{1}{2}\left(\frac{\partial U_i}{\partial x_j} - \frac{\partial U_j}{\partial x_i}\right) \tag{5}$$

The quantity $C_v = 0.5/(1 + T_t\sqrt{S^2 + W^2})$ is evaluated such that $C_v \approx C_\mu$ in the logarithmic region of a turbulent channel flow, where $T_t S = T_t W \approx 3.3$ [3].

Note that unlike the turbulence Reynolds number $Re_\mathrm{T} = k^2/v\varepsilon$, the wall-distance free parameter R_λ is defined in terms of the total kinetic energy and strain rate/vorticity invariants. In principle, no mean flow Reynolds number enters the turbulent transport equations. However, the justification herein is that the invariants η make good correspondence with the total kinetic energy K_T, thereby returning a numerically plausible formulation for the eddy viscosity damping function. In fact, it is a difficult task to devise $f_\mu = f_\mu(Re_\mathrm{T})$ that accords well with the measured and DNS data.

The empirical function f_μ is valid in the whole flow field, including the viscous sublayer and the logarithmic layer. In the region close to the wall, the Reynolds stress $-\overline{uv} \sim y^3$ and $k \sim y^2$. To preserve the correct cubic power-law behaviour of $-\overline{uv}$, the damping function needs to increase proportionally to y^{-1} in the near-wall region. Equation (4) confirms that as $y \to 0$, $R_\lambda \sim y$ and hence $f_\mu = O(C_v)$ at the close proximity of the wall (i.e. f_μ claims to increase like $f_\mu \sim y^{-1}$). As evinced by Figure 1 in comparison with the DNS data [13] for fully developed turbulent channel flows, the proposed function $f_\mu = 1$ remote from the wall to ensure that the model is compatible with the standard k–ε turbulence model. The use of R_λ confronts the singularity at neither the separating nor the reattaching point in contrast to the adoption of $y^+ = u_\tau y/v$, where u_τ is the friction velocity. Consequently, the model is applicable to separated and reattaching flows.

The budgets of k and ε from the DNS data confirm that the role of turbulent diffusion in the near-wall region is substantial. Accordingly, the Prandtl numbers σ_k and σ_ε are modelled, rather than being assigned constant values (unlike the commonly adopted practice with $\sigma_k = 1.0$ and $\sigma_\varepsilon = 1.3$):

$$\sigma_\varepsilon = C_T(4C_v + f_\sigma), \quad \sigma_k = \frac{\sigma_\varepsilon}{(1 - C_v f_\sigma)} \tag{6}$$

where $f_\sigma = f_\mu/(\sqrt{\beta} + f_\mu^3)$. The distribution of σ is depicted in Figure 1. The model coefficients σ_k and σ_ε are developed such that sufficient diffusion is obtained in the vicinity of the wall and in the core region of the flow $\sigma_k/\sigma_\varepsilon > 1$ to eliminate the common drawback where the turbulent diffusion of k overwhelms the diffusion of ε with $\sigma_k < \sigma_\varepsilon$ at [4]. Note that the

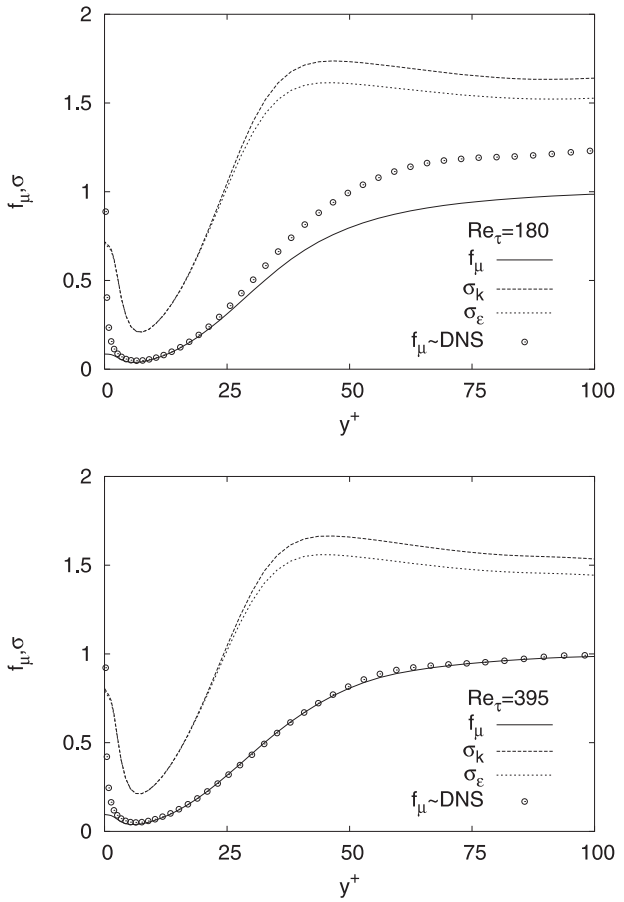

Figure 1. Variations of f_μ and σ with wall distance in channel flow.

parameters/coefficients associated with the turbulent Prandtl numbers $\sigma_{(k,\varepsilon)}$ have the values in the range from 0 to 1. For instance, $0 < f_\sigma \leqslant 1$, $0 < C_v \leqslant 0.5$ and $0 < \beta < 0.5$. Therefore, the violation of realizability and the occurrence of singularity problem in Equation (6) are out of question.

Near-wall flows show a tendency to underestimate the dissipation rate ε due to the local anisotropy of turbulence [14]. To enhance dissipation in such a situation the formulation is developed with the assistance of Reference [10] as

$$C_{\varepsilon 1} = 1 + \beta, \quad C_{\varepsilon 2} = 1.33 C_{\varepsilon 1} \tag{7}$$

It is appropriate to emphasize that the proposed relation indubitably is conducive to allowing compatible changes in both $C_{\varepsilon 1}$ and $C_{\varepsilon 2}$ that account for the additional production of dissipation by the anisotropy of turbulence. Remarkably, $C_{\varepsilon 2}/C_{\varepsilon 1} = 1.33$, converging toward the standard $C_{\varepsilon 2}$-to-$C_{\varepsilon 1}$ ratio $(1.92/1.44 \approx 1.33)$.

The extra source term E_ε in Equation (2) is constructed from the cross-diffusion model [11] as

$$E_\varepsilon = 2\,\frac{\mu_T}{T_t}\,\max\left[\frac{\partial(k/\varepsilon)}{\partial x_j}\,\frac{\partial k}{\partial x_j}, 0\right] \tag{8}$$

Obviously, the source term E_ε stimulates the energy dissipation in non-equilibrium flows, thereby reducing the departure of the turbulent length scale from its local equilibrium value and enabling improved prediction of adverse pressure gradient flows accompanied by flow separation and reattachment.

The pressure diffusion term Π_ε in Equation (2) adjusts inherently with the limit of near-wall balance in the ε equation and can be derived as [10]

$$\Pi_\varepsilon = -\frac{1}{2}\,\frac{\partial}{\partial x_j}\left(\mu\,\frac{\varepsilon}{k}\,\frac{\partial k}{\partial x_j}\right) \tag{9}$$

Essentially, the compatibility relation mimics the diffusive nature of the pressure diffusion, resembling the conventional cross-diffusion model [15]. It generates an additional source for ε in the buffer zone. To receive positive benefits from the numerical reliability in the vicinity of the wall, Equation (9) is deliberately modelled as

$$\Pi_\varepsilon \approx -\frac{1}{2}\,\frac{\partial}{\partial x_j}\left(\mu\,\frac{k\varepsilon}{C_T^2 \nu\varepsilon + k^2}\,\frac{\partial k}{\partial x_j}\right) = -\frac{1}{2}\,\frac{\partial}{\partial x_j}\left(\frac{\rho k}{2 + Re_\mathrm{T}}\,\frac{\partial k}{\partial x_j}\right) \tag{10}$$

where $C_T\sqrt{\nu\varepsilon}$ is the Kolmogorov eddy energy scale. A close look at the entire contrivance reveals that Equation (10) is equivalent to Equation (9) when $Re_\mathrm{T} \gg 2$ and $\Pi_\varepsilon = 0$ as the wall is approached. It seems likely that Π_ε is prone to loose its influence outside the close proximity of the wall due to the molecular diffusion alone, having agreement with the DNS.

3. COMPUTATIONS

To ascertain the efficacy of the proposed model, a few applications to two-dimensional turbulent flows consisting of fully developed channel flows, a flat plate boundary layer flow with zero pressure gradient, and a backward facing step flow. For a comparison purpose, calculations from the original Chien (OCH) model [5] and the modified Chien (MCH) model [6] are included. A cell-centred finite-volume scheme combined with an artificial compressibility approach [16] is employed to solve the flow equations. A fully upwinded second-order spatial differencing is applied to approximate the convective terms. A diagonally dominant alternating direction implicit (DDADI) time integration method [17] is applied for the iterative solution of the discretized equations. A multigrid method is utilized for the acceleration of convergence [18].

3.1. Channel flow

The computation is carried out for fully developed turbulent channel flows at $Re_\tau = 180$ and 395, for which turbulence quantities are attainable from the DNS data [13]. Calculations are conducted in the half-width of the channel, imposing cyclic boundary conditions except for the pressure. For both cases, the length of the computational domain is 32δ, where δ is

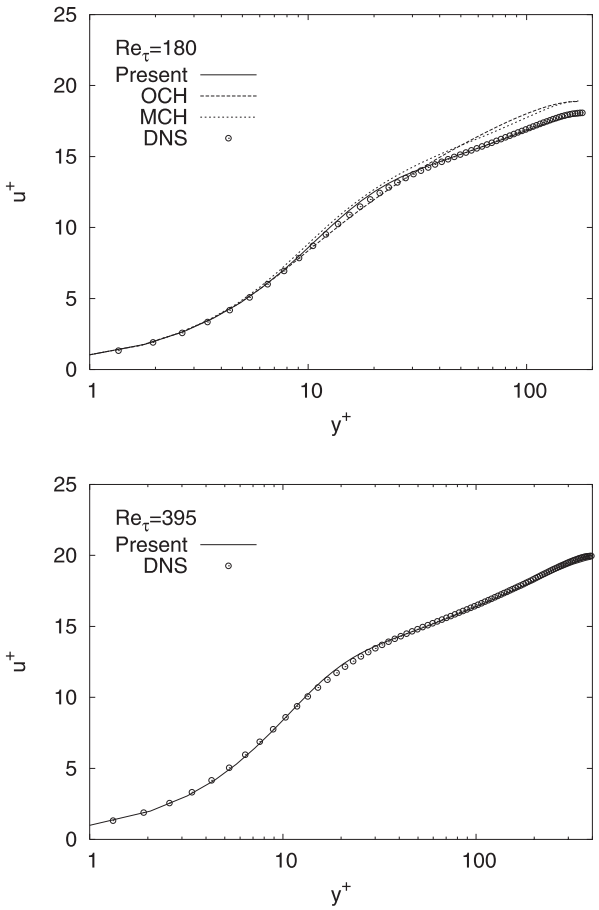

Figure 2. Mean velocity profiles of channel flow.

the channel half-width. A 96×64 non-uniform grid refinement is considered based on the grid independence test. To ensure the resolution of the viscous sublayer the first grid node near the wall is placed at $y^+ \approx 0.3$. Comparisons are made by plotting the results in wall units.

Figure 2 shows the velocity profiles for different models. Predictions of both the present and MCH models agree well with the DNS data. The OCH model slightly overestimates the mean velocity profile in the outer layer. Profiles of turbulent shear stresses are displayed in Figure 3. Agreement of all model predictions with the DNS data seems to be almost perfect.

Further examination of the model performances can be directed to the k^+ profiles as portrayed in Figure 4 for the near-wall region. As is evident, the present model prediction is in broad accord with the MCH model and DNS data. On the contrary, the OCH model predicts a peak at a slightly shifted location. Figure 5 exhibits the profiles of ε^+ from the three computations. The present model provides a maximum ε^+ at the wall which is more in line with the experimental and DNS data. In strong contrast, the OCH and MCH models indicate misplaced local maxima.

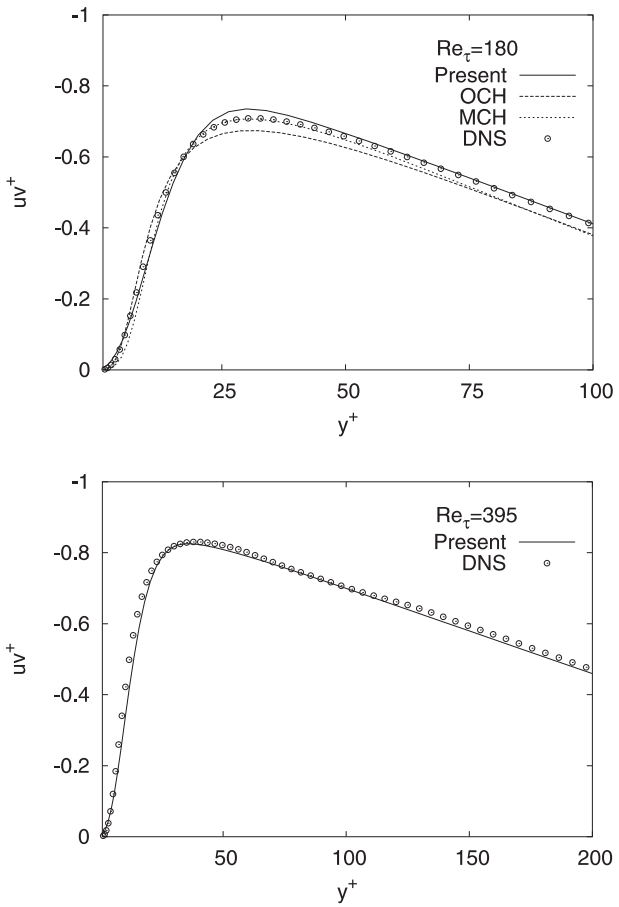

Figure 3. Shear stress profiles of channel flow.

3.2. *Flat plate boundary layer flow*

The performance of the proposed model is further contrasted with the experimental data of the flow over a flat plate with a high free stream turbulence intensity. The test case is taken from 'ERCOFTAC' Fluid Dynamics Database WWW Services (http://fluindigo.mech.surrey.ac.uk/) preserved by P. Voke. Measurements down to $x = 1.495$ m which corresponds to $Re_x \approx 94\,000$, are made by J. Coupland at Rolls-Royce. The inlet velocity is 9.4m/s and the pressure gradient is zero. The upstream turbulence intensity $T_u = 6.0\%$, defined as $T_u = \sqrt{\frac{2}{3}k}/U_{\text{ref}}$, where U_{ref} indicates the reference velocity. The dissipation is set so that the decay of free stream turbulence is in balance.

Computations begin 16 cm ahead of the leading edge and symmetric conditions are applied. The length and height of the grid are 1.6 and 0.3 m, respectively. The near-wall grid node is located at $y^+ < 1.0$, except the point at the leading edge ($y^+ = 2.1$). The grid size is 96×64 and heavily clustered near the wall.

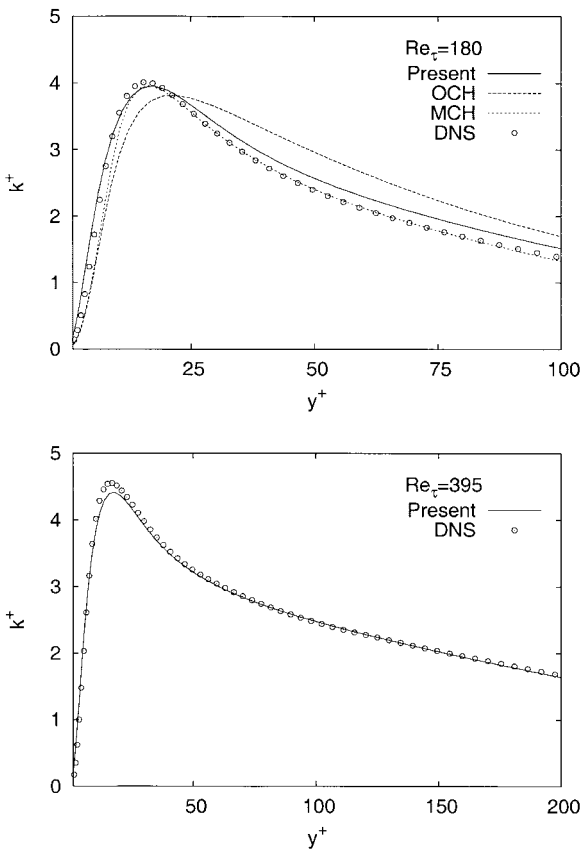

Figure 4. Turbulence kinetic energy profiles of channel flow.

The predicted skin friction coefficients are compared with the experimental data in Figure 6. The overall performance in predicting the friction coefficient is the best for the present model, exhibiting an interesting feature that the transition starts at the right position and it is strong enough. In contrast, both the OCH and MCH models, having the wall distance in the damping functions provide earlier transition than that seen in the experiment. Seemingly, the agreement between the computations and the experiment is fairly good toward the end of the transition (e.g. beyond $x = 0.195\,\mathrm{m}$). However, the MCH model prediction is somewhat on a lower level than the data show.

3.3. Backward facing step flow

To validate the performance in complex separated and reattaching turbulent flows, the present model is applied to the flow over a backward facing step flow. The computation is conducted corresponding to the experimental case with zero deflection of the wall opposite to the step, as investigated by Driver and Seegmiller [19]. The ratio between the channel height and the step height h is 9, and the step height Reynolds number is $Re = 37\,500$. At the channel inlet, the

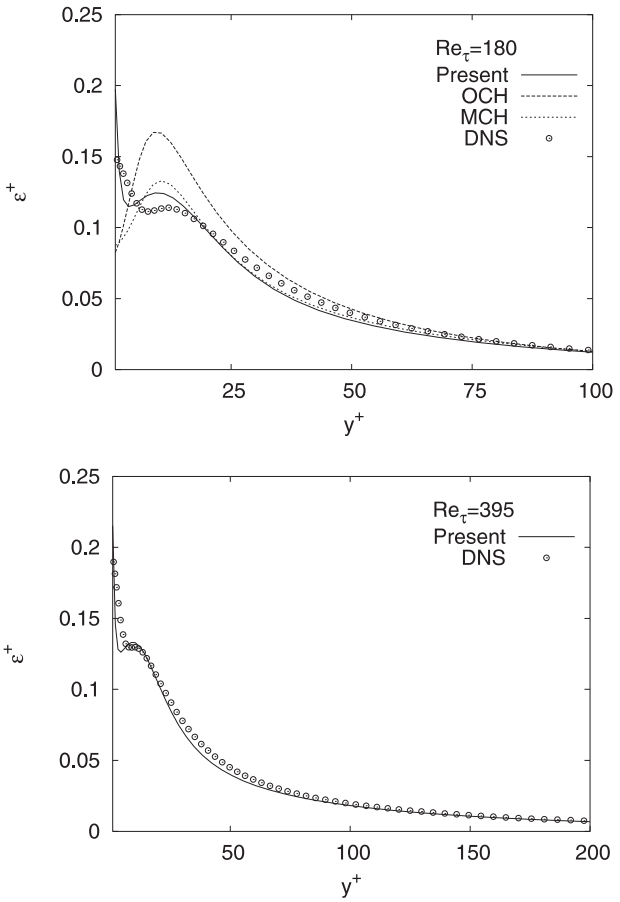

Figure 5. Dissipation rate profiles of channel flow.

Reynolds number based on the momentum thickness is $Re_\theta = 5000$. A 128×128 non-uniform grid is used for the computations and the maximum height of the first near-wall grid node is at $y^+ < 1.5$. The distance x/h shown below is measured exactly from the step corner.

The inlet profiles for all dependent variables are generated by solving the models at the appropriate momentum thickness Reynolds number. Profiles of mean velocity, shear stress and turbulent kinetic energy at inlet are presented in Figure 7. The MCH and present models ensure close adherence to the experimental data. The OCH model predicts the velocity field which is in fair agreement with the measurement. However, this model exhibits some discrepancies between the predictions and the data for the shear stress and turbulent kinetic energy profiles, especially in near-wall regions.

Computed and experimental friction coefficients C_f along the step side wall are plotted in Figure 8. As is observed, the OCH model gives the C_f distribution with a large overshoot followed by a sudden drop in the immediate vicinity of the reattachment point. The positive C_f that starts from $x/h = 0$, is due to a secondary eddy which sits in the corner at the base of

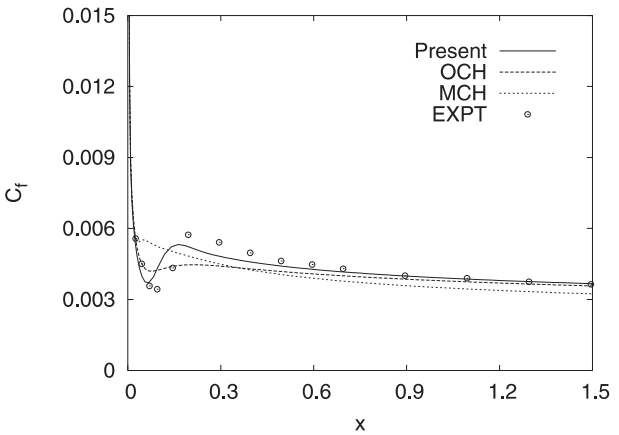

Figure 6. Streamwise skin friction coefficient of boundary layer flow.

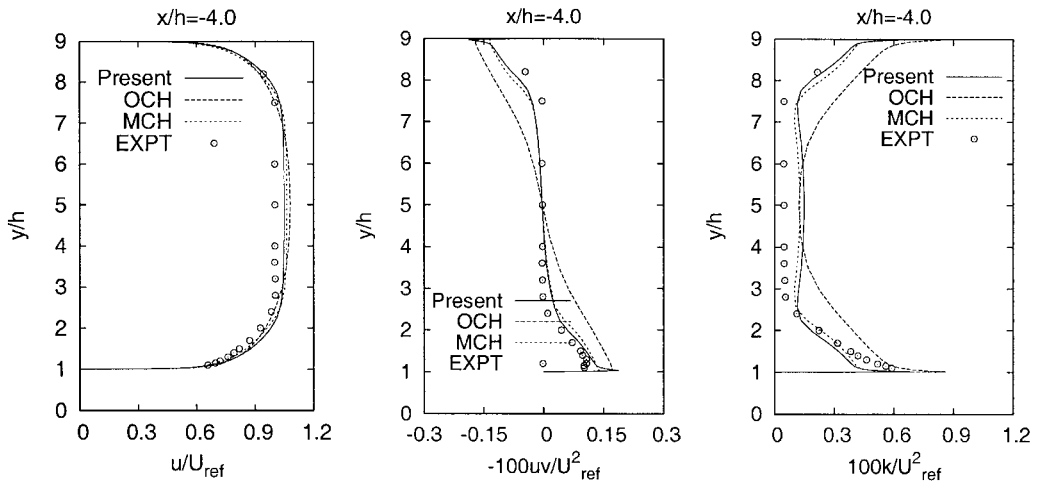

Figure 7. Inlet profiles for step flow.

the step, inside the main recirculation region. The OCH model predicts a recirculation length of 5.4. The corresponding predictions by the MCH and present models are 6.8 and 6.23, respectively. The experimental value of the reattachment length is 6.26 ± 0.1, making a fairly good correspondence with the present and MCH models.

The streamwise mean velocity profiles at four representative positions are depicted in Figure 9. Obviously, the predictions of all models are in good agreement with the experiment. It is a bit nebulous that the inaccurate prediction of the C_f distribution by the OCH model has little effect on the velocity profiles. Comparisons are extended to the distributions of the Reynolds shear stress and the corresponding turbulent kinetic energy at different x/h locations behind the step corner, as shown in Figures 10 and 11. A closer inspection of the

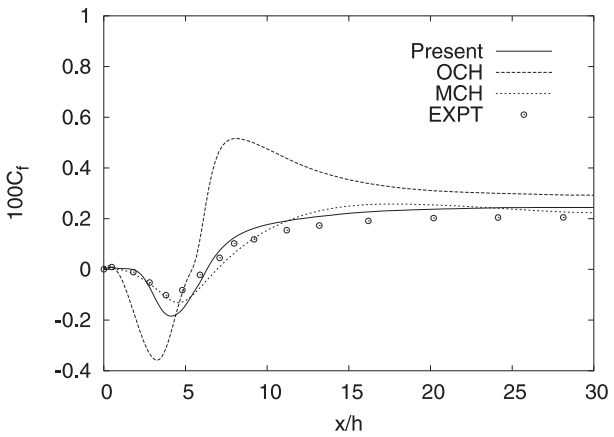

Figure 8. Skin friction coefficient along the step-side bottom wall.

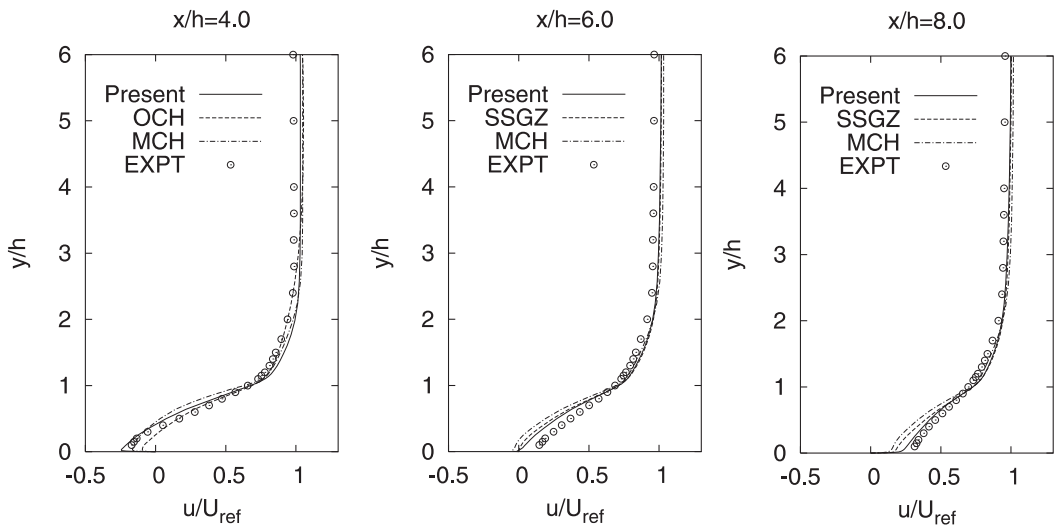

Figure 9. Mean velocity profiles at selected locations for step flow.

distribution indicates that the present model predictions are in a broad agreement with the experimental data. On average, the agreement is good in both the recirculation and recovery regions.

4. CONCLUSIONS

The proposed turbulent model is wall-distance-free, tensorially invariant and frame-indifferent. Consequently, it is applicable to arbitrary topologies in conjunction with structured or

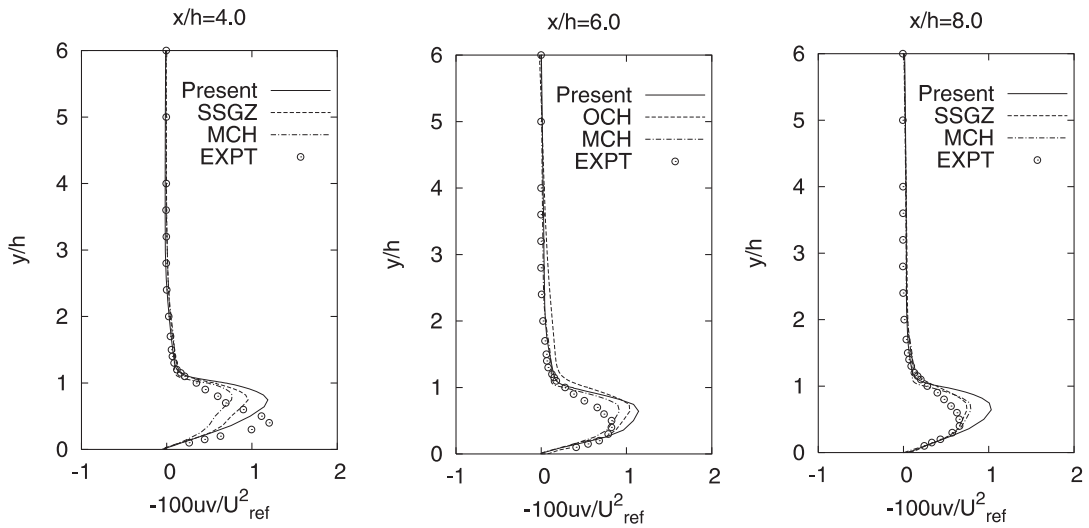

Figure 10. Shear stress profiles at selected locations for step flow.

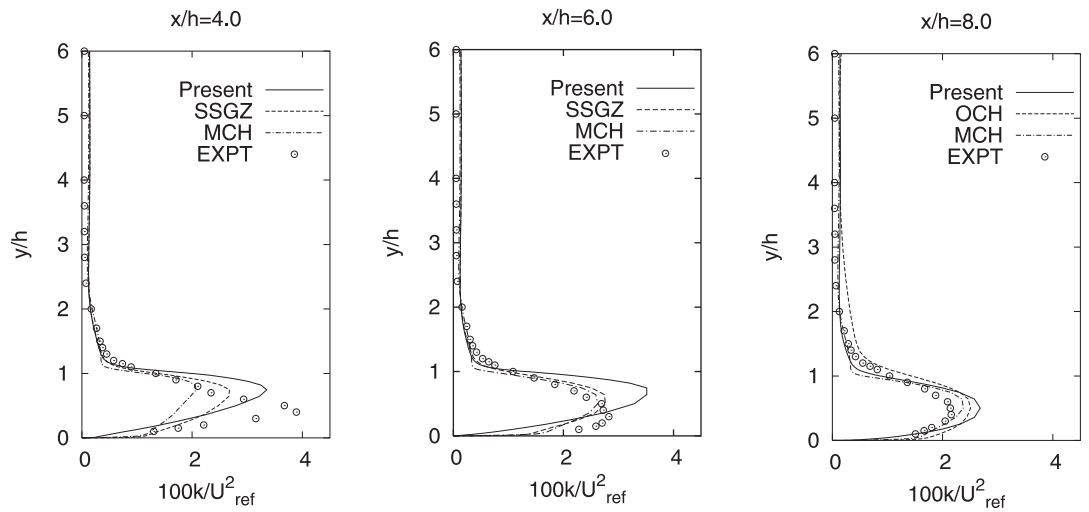

Figure 11. Kinetic energy profiles at selected locations for step flow.

unstructured grids. The model accounts for the distinct effects of low Reynolds number and wall proximity. The potential importance of the damping functions is conspicuous. The anisotropic production in the dissipation equation is accounted for substantially by modifying the model constants $C_{\varepsilon(1,2)}$ and adding cross-diffusion terms. The model is capable of evaluating the flow case entangling separation and reattachment.

NOMENCLATURE

C_f	friction coefficient
C_μ	eddy viscosity coefficient
E_ε	source term in dissipation equation
f_μ, f_σ	viscous damping functions
h	step height
k	turbulent kinetic energy
K_T	total kinetic energy
P	turbulent production term
Re_T	turbulent Reynolds number
R_λ	wall-distance free parameter
S	mean strain rate invariant
T_t	realizable time scale
T_u	turbulence intensity
t	time
$-\overline{u_i u_j}$	Reynolds stresses
U_i	mean velocity components
U_{ref}	reference velocity
W	mean vorticity invariant
x_i	Cartesian co-ordinates
y^+	non-dimensional normal distance from wall

Greek letters

β	turbulent anisotropy
ε	turbulent dissipation
μ, μ_T	laminar and eddy viscosities
ν	molecular kinematic viscosity
ρ	density
Π_ε	pressure diffusion term
σ	turbulent Prandtl number

REFERENCES

1. Patel VC, Rodi W, Scheuerer GG. Turbulence models for near-wall and low Reynolds number flow: a review. *AIAA Journal* 1985; **23**:1308–1319.
2. Nagano Y, Kondoh M, Shimada M. Multiple time scale turbulence model for wall and homogeneous flows based on direct numerical simulations. *International Journal of Heat and Fluid Flow* 1997; **18**:346–359.
3. Rahman MM, Rautaheimo P, Siikonen T. Modifications for an explicit algebraic stress model. *International Journal for Numerical Methods in Fluids* 2001; **35**:221–245.
4. Nagano T, Tagawa M. An improved k–ε model for boundary layer flows. *Journal of Fluids Engineering* 1990; **112**:33–39.
5. Chien K-Y. Predictions of channel and boundary layer flows with a low-Reynolds number turbulence model. *AIAA Journal* 1982; **20**(1):33–38.
6. Rahman MM, Siikonen T. Improved low-Reynolds-number k–$\tilde{\varepsilon}$ model. *AIAA Journal* 2000; **38**(7):1298–1300.
7. Jones WP, Launder BE. The calculation of low-Reynolds number phenomena with a two-equation model of turbulence. *International Journal of Heat Mass Transfer* 1973; **16**:1119–1130.
8. Goldberg U, Apsley D. A wall-distance-free low RE k–ε turbulence model. *Computer Methods in Applied Mechanics and Engineering* 1997; **145**:227–238.

9. Rahman MM, Siikonen T. Low-Reynolds-number k–$\tilde{\varepsilon}$ model with enhanced near-wall dissipation. *AIAA Journal* 2002; **40**(7):1462–1464.
10. Rahman MM, Siikonen T. Near-wall turbulence modelling with enhanced dissipation. *International Journal for Numerical Methods in Fluids* 2003; **42**:979–997.
11. Rahman MM, Siikonen T. A new time scale based low-Re k–ε model. In *The 3rd International Conference on Computational Heat and Mass Transfer*, Banff, Canada, Mohamad AA (ed.). Calgary University Press: Alberta, 2003; 754–763.
12. Bradshaw P. Turbulence modeling with application to turbo-machinery. *Progress in Aerospace Science* 1996; **32**:575–624.
13. Mansour NN, Kim J, Moin P. Reynolds-stress and dissipation-rate budgets in a turbulent channel flow. *Journal of Fluid Mechanics* 1988; **194**:15–44.
14. Durbin PA, Speziale CG. Local anisotropy in strained at high Reynolds numbers. *Journal of Fluids Engineering* 1991; **113**:707–709.
15. Yoshizawa A. Statistical modeling of a transport equation for the kinetic energy dissipation rate. *Physics of Fluids A* 1987; **30**(3):628–631.
16. Rahman MM, Siikonen T. An artificial compressibility method for incompressible flows. *Numerical Heat Transfer*, *Part B* 2001; **40**:391–409.
17. Lombard C, Bardina J, Venkatapathy E, Oliger J. Multi-dimensional formulation of CSCM—an upwind flux difference eigenvector split method for the compressible Navier–Stokes equations. In *Sixth AIAA Computational Fluid Dynamics Conference*, *AIAA Paper 83-1895-CP*, 1983; 649–664.
18. Jameson A, Yoon S. Multigrid solution of the Euler equations using implicit schemes. *AIAA Journal* 1986; **24**:1737–1743.
19. Driver DM, Seegmiller HL. Features of a reattaching turbulent shear layer in divergent channel flow. *AIAA Journal* 1985; **23**(2):163–171.

